https://doi.org/10.1016/j.ijhydene.2022.09.007

A bifunctional electrochemical flow cell integrating ammonia production and electricity generation for renewable energy conversion and storage

Zhefei Pan[a], Yun Liu[a], Zhewei Zhang[a], Zhen Zhao[a], Jie Zhu[b,*], Rong Chen[c,d,*], Liang An [a,e,*]

[a] Department of Mechanical Engineering, The Hong Kong Polytechnic University, Hung Hom, Kowloon, Hong Kong SAR, China

[b] Institute of Acoustics, School of Physics Science and Engineering, Tongji University, Shanghai 200092, China

[c] Key Laboratory of Low-grade Energy Utilization Technologies and Systems (Chongqing University), Ministry of Education, Chongqing 400030, China

[d] Institute of Engineering Thermophysics, Chongqing University, Chongqing 400030, China

[e] The Hong Kong Polytechnic University Shenzhen Research Institute, Shenzhen 518057, China

*Corresponding authors.

Email: jiezhu@tongji.edu.cn (Jie Zhu)

Email: rchen@cqu.edu.cn (Rong Chen)

Email: liang.an@polyu.edu.hk (Liang An)

Abstract

Renewable energy has rapidly advanced in the global energy system, triggering the visible development of energy storage technologies in recent decades. Among them, the electricity-fuel-electricity approach is an effective way for the storage and utilization of renewable power. In this work, a bifunctional electrochemical flow cell integrating both ammonia production and electricity generation modes is developed for renewable energy conversion and storage. Ammonia, a hydrogen carrier having a high hydrogen content of 17.6 wt. %, is relatively easier to convert to liquid phase for large-scale storage. The long-distance ammonia transport can

reliably depend on the established infrastructure. In addition, as a carbon-free fuel beneficial for achieving the goal of carbon-neutrality, ammonia is considered as an environmentally benign and cost-effective mediator fuel. This flow cell is able to operate via two modes, i.e., an ammonia-production mode for energy storage in the form of ammonia (via nitrogen reduction reaction) and an electricity-generation mode for energy conversion in the form of electricity (via ammonia oxidation reaction). This flow cell is constituted by a PtAu/C-coated nickel-foam electrode for nitrogen and oxygen reduction reactions, a Pt/C-coated nickel-foam electrode for water and ammonia oxidation reactions, and an alkaline anion exchange membrane for charge-carrier migration. Charging this flow cell with the supply of nitrogen results in a Faradaic efficiency of 2.70% and an ammonia production rate as high as 9.34×10^{-10} mol s^{-1} cm^{-2} at 23 °C. Moreover, energizing this flow cell with ammonia results in an open-circuit voltage of 0.59 V and a peak power density of 3.31 mW cm^{-2} at 23 °C. A round-trip efficiency of 25.7% is realized with the constant-electrode mode.

Keywords: Renewable energy; Energy conversion and storage; Electrochemical flow cell; Ammonia mediator; Operation mode

1. Introduction

The world has witnessed a significant increase on the global energy use and demand over the past few decades with this trend expected to continue in the future [1, 2]. Currently, energy utilization and power generation are mainly carried out through fossil fuels, whereas this kind energy resource would result in a great deal of harmful emissions to the air [3, 4]. Therefore, it has been joint global attention and efforts to reduce the participation of the fossil fuels in the modernized way of energy utilization and power generation [5, 6]. Among the thoughts of improvement, the electricity-fuel-electricity approach realized by a bifunctional electrochemical flow cell has been come up with, which can be used as both fuel-production mode and electricity-generation mode [7, 8]. The fuel-production mode is capable of converting renewable energy that are however intermittent and unreliable into chemical energy stored in fuels to secure an efficient and stable supply of electricity, wherever and whenever the electricity is demanded [9]. The renewable electricity is able to be generated through the electricity-generation mode, which is a promising method to realize the environmentally friendly energy utilization [10, 11]. This reversible system exhibits several distinctive advantages, including non-pollution emission, high specific energy, no self-discharge, and decoupled energy storage capacity with rated power [12]. In addition, this system has the superiority of mass and volume savings, hence possessing the potential to be applied in energy systems for a wider range of fields and scenarios [13].

Currently, the most common bifunctional electrochemical flow cell is running on the mediator fuel of hydrogen [14, 15]. Hydrogen, a carbon-free and environmental-benign fuel, is a promising candidate fuel that could reduce the pollution derived from fossil fuels [16]. In addition, the high energy density makes it an excellent energy carrier [17]. In the conventional system, water is spilt into hydrogen and oxygen driven by the renewable electricity initially to store renewable energy, and reversely, the hydrogen and oxygen are fed as the fuel and oxidant,

respectively, to generate electricity once demanded and form water to complete the cycle [18, 19]. However, the use of hydrogen as the mediator fuel faces various challenges. Since hydrogen is the lightest gas, the storage of hydrogen is one of the main challenges, which requires compression and liquefaction of hydrogen gas at low temperatures and high pressures (1.3 MPa at -239.96 ºC) [20]. The infrastructures for transporting hydrogen for long distance and storing hydrogen for long term have not been established, which demand high up-front costs [21]. Further, due to its highly flammable nature, hydrogen may create a series of safety issues [22].

To address these challenges in the use of hydrogen as the mediator fuel, in this work, the ammonia is selected as a promising alternative to serve as the mediator fuel for bifunctional systems. Ammonia, a hydrogen carrier having a high hydrogen content of 17.6 wt. %, has several advantages over hydrogen [23]. The boiling temperature of ammonia at ambient pressure is -33.4 ºC, such that it is relatively easier to be converted to liquid phase for large-scale storage [24]. The long-distance ammonia transport can reliably depend on the established infrastructures. Also, ammonia has a higher energy (4 $kWh\,kg^{-1}$). Besides, ammonia has a narrow flammability range (16-25% by volume in air), which reduces the security risks associated with hydrogen [25]. Finally, as a carbon-free fuel beneficial for achieving the goal of carbon-neutrality, ammonia is considered as an environmentally benign and cost-effective mediator fuel [26].

A bifunctional electrochemical flow cell mediated by ammonia capable of converting and storing renewable energy in an electricity-fuel-electricity approach is demonstrated. This process is realized through an electrochemical flow cell with two operation modes, i.e., a fuel-production mode for energy storage in the form of ammonia (via nitrogen reduction reaction) and an electricity-generation mode for energy conversion in the form of electricity (via ammonia oxidation reaction). The fuel-production mode is able to use renewable electricity to

convert nitrogen and water into ammonia, and simultaneously achieve the long-term energy storage in the form of ammonia. The electricity-generation mode is capable of generating power via oxidizing ammonia into nitrogen and water, and converting chemical energy stored in ammonia directly into electricity. Charging the flow cell, constituted by a PtAu/C-coated nickel-foam electrode for nitrogen and oxygen reduction reactions, a Pt/C-coated nickel-foam electrode for water and ammonia oxidation reactions, and an alkaline anion exchange membrane (AEM) for charge-carrier migration, results in a Faradaic efficiency of 2.70% and an ammonia production rate as high as 9.34×10^{-10} mol s^{-1} cm^{-2} at 23 °C. Moreover, energizing the flow cell results in an open-circuit voltage (OCV) of 0.59 V and a peak power density of 3.31 mW cm^{-2} at 23 °C.

2. Working principle

A typical schematic of bifunctional electrochemical flow cell mediated by ammonia is depicted in Fig. 1. The system consists of a membrane electrode assembly (MEA) fabricated by a cathode, an AEM, an anode, and two flow fields. In the ammonia-production mode, the potassium hydroxide (KOH) solution is supplied to the anode flow field. With the voltage applied, oxygen evolution reaction (OER) takes place and releases electrons as the forward reaction in Eq. 1 [27]:

$$6OH^- \leftrightarrow \frac{3}{2}O_2 + 6e^- + 3H_2O \qquad E^0 = 0.4 \text{ V vs. SHE} \tag{1}$$

The electrons generated by the OER are transported through an external circuit to the cathode. Subsequently, nitrogen entering the cathode flow field combines with the electrons and participates in the nitrogen reduction reaction (NRR) that produces ammonia as the forward reaction in Eq. 2 [28]:

$$N_2 + 6H_2O + 6e^- \leftrightarrow 2NH_3 + 6OH^- \qquad E^0 = -0.77 \text{ V vs. SHE} \tag{2}$$

Meanwhile, the internal ion circuit is formed by the hydroxide-ion migration through the AEM. The overall reaction of ammonia-production mode is shown as the forward reaction in Eq. 3:

$$N_2 + 3H_2O \leftrightarrow 2NH_3 + \frac{3}{2}O_2 \qquad E^0 = 1.17\ V \tag{3}$$

The products of ammonia and oxygen from the ammonia-production mode could serve as the reactants in the electricity-generation mode, thus creating a reversible system. In the electricity-generation mode, the anolyte containing ammonia and KOH is fed into the anode flow filed, and ammonia oxidation reaction (AOR) happens on the anode, producing nitrogen, water and electrons as the backward reaction in Eq. 1 [29]. The electrons generated by the AOR are transported through an external circuit to the cathode. Subsequently, oxygen entering the cathode flow field combines with the electrons and participates in the oxygen reduction reaction (ORR) that produces hydroxide ions as the backward reaction in Eq. 2 [30]. Meanwhile, the internal ion circuit is formed by the hydroxide-ion migration through the AEM. The overall reaction of electricity-generation mode is shown the backward reaction in Eq. 3. With the combination of two operation modes, this bifunctional flow cell mediated by ammonia will provide a significant solution for the renewable energy conversion and storage.

3. Experimental section

3.1. Materials

Pt/C was bought from Johnson Matthey (UK). Gold(III) chloride trihydrate powder was bought from Sigma-Aldrich (USA). Nickel foam was bought from Hohsen Co. (Japan). Fumasep series membranes were purchased from Fuel Cell Store (USA).

3.2. Preparation of PtAu/C

The PtAu/C nanoparticles was synthesized by a chemical reduction using sodium borohydride ($NaBH_4$) as the reducing agent [31]. First, 30.0 mg 60 wt. % Pt/C was dispersed in 300.0 mL of water and ultrasonically stirred for 30 min. Then a solution of 2.5 mL sodium citrate (0.2 mol L^{-1}) as the stabilizing agent was added to the solution. The mixed solution was magnetically stirred for 30 min. Afterwards, a solution of 100.0 mL $NaBH_4$ (0.5 mmol) was poured into the mixed solution. Then 3.6 mL of chloroauric acid ($HAuCl_3$) solution (25 mmol

L^{-1}) was diluted in 100.0 mL and the pH was adjusted to 4.0. Subsequently, the diluted solution was added to the as-prepared mixed solution. After magnetically stirring for 12 h, the solution was filtered with filter paper, washed with excessive hot water, and then dried in air at 23 ºC for 8 h. Finally, the PtAu/C had a metal content of 75% and a Pt:Au ratio of 1:1.

3.3. Characterization of PtAu/C

The morphology of PtAu/C was characterized by scanning electron microscopy (SEM) (Tescan VEGA3, Czech) and transmission electron microscopy (TEM) (JEOL Model JEM-2100F, Germany). X-ray diffraction (XRD) data were recorded on a diffractometer (Rigaku SmartLab, Japan). X-ray photoelectron spectroscopy (XPS) analysis was performed on an X-ray photoelectron spectrometer (Thermo Scientific Nexsa, USA) using aluminum Kα radiation as the exciting source.

3.4. Preparation of a membrane electrode assembly

Nickel foam was used as the substrate for electrodes in the flow cell. The electrodes were prepared by a dip-coating method [32]. First, carbon supported catalyst, 5 wt. % Nafion solution and ethanol were mixed to obtain the catalyst ink. Afterwards, the ink was ultrasonically stirred for 30 min to well disperse it. Then the nickel foam was dipped in the ink for 1 min and dried by a blower. The dipping and drying were repeated 10 times and the catalyst coated on the nickel foam each time was roughly determined by the weight difference. When the catalyst loading was approaching the set value, the weight was measured every dipping-drying cycle to prevent the overloaded loading. Finally, the dipping and drying were repeated until the catalyst loading reached the set value. The electrode was cut to the desired area of 2.0 cm × 2.0 cm. The MEA consisted of a piece of Pt/C coated nickel foam, a pre-treated Fumasep membrane (Fuel Cell Store, USA), and a piece of PtAu/C coated nickel foam. The Fumasep membrane with an area of 3.0 cm × 3.0 cm was immersed in 1.0 M KOH solution at 23 ºC for 24 h.

3.5. Cyclic voltammetry, linear sweep voltammetry and chronoamperogram

Cyclic voltammetry (CV) was conducted in a single-chamber electrochemical cell at 23 ºC. The as-prepared electrodes, a Pt foil and a silver/silver chloride electrode were used as the working electrode, counter electrode and reference electrode, respectively. The electrolytes were 1.0 M KOH solution in the absence and presence of 1.0 M NH_3. The potential window for the CV tests was from -0.8 V to 0.8 V at a scan rate of 50 mV s^{-1}. Linear sweep voltammetry (LSV) was conducted in a H-type electrochemical cell. The as-prepared electrodes, a graphite rod and a silver/silver chloride electrode were used as the working electrode, counter electrode and reference electrode, respectively. The electrolytes in both chambers were 1.0 M KOH solution with continuous bubbling of argon or nitrogen gas. The potential window for the LSV tests was from 0 V to -1.3 V at a scan rate of 2.5 mV s^{-1}. The chronoamperogram (CA) tests of the Pt/C and PtAu/C were conducted in Ar-saturated 1.0 M KOH with 0.1 M NH_3 at 0.10 V vs Ag/AgCl under ambient conditions. The CV, LSV and CA curves were recorded by an electrochemical workstation (PGSTAT302N, Switzerland).

3.6. Flow cell setup and instrumentation

A home-made fixture was used to fabricate the electrochemical flow cell with a single serpentine flow field. To avoid electrolyte leakage, polytetrafluoroethylene (PTFE) gaskets were added between two half fixtures. The polarization curves of charging and discharging processes were recorded by an Arbin BT2000 (Arbin instrument Inc., USA).

3.7. Ammonia determination

The ammonia concentration was determined by the indophenol blue method [33]. 1.0 mL sample solution was mixed with 1.0 mL solution consisting salicylic acid, sodium citrate, and 1.0 M NaOH, 0.5 mL solution of sodium hypochlorite, and 0.1 mL solution of sodium nitroferricyanide dihydrate in sequence. The final solution was maintained for 2 h, then it was tested by a UV-vis spectrometer.

4. Results and discussion

4.1. Characterization of PtAu/C

The SEM image of PtAu/C in Fig. 2 shows that the Pt and Au elements are uniformly distributed on the carbon particles, which contributes to the exposure of active sites for electrochemical reactions. Fig. 3 shows the XRD pattern of PtAu/C, and the main diffraction peaks assigned to the (111), (200), (220), (311) and (222) facets are observed at 38.6º, 44.5º, 64.6º, 77.5º and 81.5º for Au element, as well as 39.6º, 46.3º, 67.6º, 81.5º and 85.9º for Pt element [34]. The major (111) and (200) facets of both Au and Pt are further revealed by TEM images. The interlayer spacings of 0.235 nm and 0.225 nm in Fig. 4a correspond to the (111) facets of Au and Pt, respectively. In addition, the interlayer spacings of 0.202 nm and 0.195 nm in Fig. 4b correspond to the (200) facets of Au and Pt, respectively. These results are consistent with XRD pattern. Fig. 5 shows the XPS spectra of the PtAu/C. The binding energies of 71.48 eV and 74.68 eV correspond to the Pt $4f_{7/2}$ and Pt $4f_{5/2}$, each of which can be separated into two peaks at around 71.28 eV and 72.08 eV, as well as 74.68 eV and 75.58 eV, indicating the presence of metallic Pt^0 and Pt^{2+} species [35]. From their peak intensity, Pt^0 is the predominant species. The binding energies of 84.08 eV and 87.78 eV correspond to the Au $4f_{7/2}$ and Au $4f_{5/2}$, confirming the zero-valent state of Au [36]. The above characterization results demonstrate the successful synthesis of PtAu/C in this work.

4.2. Characterization of PtAu/C-based and Pt/C-based electrodes

Fig. 6 shows the SEM images of PtAu/C-based and Pt/C-based three-dimensional electrodes. It can be seen that the skeleton of nickel foam is coated by a thin film of catalyst to form a porous structure. With this structure, the pores and channels can serve as the mass transport pathways, and the active sites on catalyst can be exposed and accessed by the reactants, to trigger the electrochemical reactions.

The CV of PtAu/C-based and Pt/C-based electrodes in 1.0 M KOH is shown in Fig. 7a. The locations of anodic and cathodic peaks are identical, but the current densities of Pt/C-based electrode are higher than those of PtAu/C-based electrode. This is because that the total metal loading of two electrodes is kept same as 1.0 mg cm^{-2}, indicating that the content of platinum in the PtAu/C-based electrode is lower than that of Pt/C-based electrode. The hydrogen adsorption and desorption peaks can be found in the potential region of -0.8 V to -0.5 V. Pt/C exhibits an increase in the current density in the double layer compared with PtAu/C, due to the formation of more platinum oxide species. The cathodic peak at around -0.35 V is attributed to the reduction of platinum oxide species. The CV of PtAu/C-based and Pt/C-based electrodes in 1.0 M ammonia and 1.0 M KOH is shown in Fig. 7b. The hydrogen desorption/sorption region is significantly suppressed in the presence of ammonia in the solution. Due to the higher platinum loading, the Pt/C-based electrode yields higher current densities in anodic scan, suggesting the it processes better AOR activity than the PtAu/C-based electrode. According to these results, the Pt/C-based electrode is preferred to serve as the anode in the electricity-generation mode, such that the PtAu/C-based electrode works as the cathode.

The ability of two electrodes towards nitrogen reduction is investigated by the LSV tests under nitrogen or argon supply. The maximum current gap between the curves can be a theoretical indicator for the nitrogen reduction ability. It is seen from Fig. 8 that the current gaps of Pt/C-based electrode and PtAu/C-based electrode are 1.85 mA cm^{-2} and 1.34 mA cm^{-2}, respectively, indicating that Pt/C-based electrode will have a higher ammonia yield when two electrodes are operated at the optimal potentials. In addition to the ammonia yield, the Faradaic efficiency is another critical index to evaluate the nitrogen reduction performance of electrodes. If two electrodes are operated at -1.09 V when the Pt/C-based electrode shows the highest ammonia yield, the Faradaic efficiencies are similar at around 10.2%. When two electrodes are operated at -1.18 V when the PtAu/C-based electrode shows the highest ammonia yield, the Faradaic

efficiency of PtAu/C-based electrode is 6.7%, higher than that of Pt/C-based electrode (2.0%). The CA results show that both catalysts exhibit promising stability.

4.3. Characterization of the flow cell mediated by ammonia

It is common that the electrode-scale characterization results obtained by the three-electrode system are not always consistent with the cell-scale characterization results, because each operation environment is radically different. Considering this effect, this section conducts the cell-scale characterization of this flow cell mediated by ammonia.

4.3.1. Effect of the catalyst on ammonia production rate

The effect of catalyst on the ammonia production is investigated to determine the optimal electrode for NRR. The anode remains the Pt/C electrode with a catalyst loading of 1.0 mg cm^{-2} and the membrane is pretreated Fumasep FAS-50. The catalyst loading on the cathode is the same as the anode with a value of 1.0 mg cm^{-2}. As shown in Fig. 9, for the Pt/C-based electrode, the ammonia production is found to be 1.14×10^{-10} mol s^{-1} cm^{-2} with a Faradaic efficiency of 0.33%. In comparison, the PtAu/C-based electrode produces the ammonia at a rate of 9.34×10^{-10} mol s^{-1} cm^{-2} while the Faradaic efficiency comes to 2.70% on this condition. The superior Faradaic efficiency of PtAu/C-based electrode in the cell-scale characterization is consistent with the electrode-scale characterization, which is attributed to the faster kinetics of hydrogen evolution reaction on Pt, resulting in the severer side reaction of hydrogen evolution [37]. On the contrary, PtAu/C-based electrode also realizes a higher ammonia production rate. This phenomenon can be ascribed to two reasons. On one hand, the cell is operated at a constant applied current density, such that the potential applied on the cathode may not reach the optimal value in the electrode-scale characterization. On the other hand, the cathode in the flow cell is fed with nitrogen gas, which completely differs from the electrode immersing in liquid solution in the electrode-scale characterization.

4.3.2. Effect of the applied current density on ammonia production rate

To study the effect of the applied current density on the ammonia production, experiments are conducted under a set of applied current densities of 5.0, 10.0, 20.0, 30.0, 40.0 and 50.0 mA cm^{-2}. The Fig. 10 displays the ammonia production rate and Faradaic efficiency with respect to the applied current density. For the experiment setup, the PtAu/C-based electrode is employed as the cathode due to its better performance as proved in section 4.3.1, and thus the Pt/C-based electrode is used as the anode. The membrane, anolyte solution and flow rate of nitrogen are kept same. With the applied current density of 5.0, 20.0, 30.0, 40.0, and 50.0 mA cm^{-2}, the ammonia production rates are 4.76, 4.97, 4.69, 4.40 and 3.93×10^{-10} mol s^{-1} cm^{-2}, respectively. Particularly, when the applied current density is 10.0 mA cm^{-2}, the ammonia production rate reaches a maximum value of 9.34×10^{-10} mol s^{-1} cm^{-2}. Regarding the Faradaic efficiency, it has the highest value of 2.75% at 5.0 mA cm^{-2}. While applying a current density of 10.0 mA cm^{-2}, the Faradaic efficiency changes subtly to 2.70%. Increasing the applied current density from 10.0 mA cm^{-2}, the Faradaic efficiency experienced a drastic falling and becomes 0.72% when the applied current density is 20 mA cm^{-2}. The Faradaic efficiency continues to decrease to 0.45%, 0.32% and 0.23% with 30.0, 40.0 and 50.0 mA cm^{-2} applied. These results can be explained as follows. When the flow cell is charged, nitrogen at the cathode will receive electrons, a necessitated reactant for NRR, and will be combined with water to produce ammonia. The maximum production rate of ammonia at 10.0 mA cm^{-2} is attributed to the sufficient electron supply, which enhances ammonia production. Nonetheless, keeping increasing of the current density, the hydrogen evolution becomes severer, resulting in the decrease of the ammonia production rate even though more electrons are provided.

4.3.3. Effect of the nitrogen flow rate on ammonia production rate

By setting a set of nitrogen flow rates of 20.0, 50.0 and 100.0 SCCM, the effect of nitrogen flow rate on the ammonia production is determined. Meanwhile, other conditions are unchanged. It is seen from Fig. 11 that when a nitrogen flow rate of 50.0 SCCM is applied, the

ammonia production rate reaches a maximum of 9.34×10^{-10} mol s^{-1} cm^{-2} and the Faradaic efficiency is 2.75% on this condition. The ammonia production rate has a value of 3.55×10^{-10} mol s^{-1} cm^{-2} with a nitrogen flow rate of 20.0 SCCM, accompanying a Faradaic efficiency of 1.03%. When the nitrogen flow rate is set to be 100.0 SCCM, the ammonia production rate becomes 6.59×10^{-10} mol s^{-1} cm^{-2} while the Faradaic efficiency becoming 1.91%. Increasing the flow rate from 20.0 SCCM to 50.0 SCCM, it is conducive for boosting the ammonia production, which is attributed to the sufficient supply of nitrogen and water, whereas a higher nitrogen flow rate beyond 50.0 SCCM will conversely decreases the ammonia production rate. It has relationships with the following two factors. Firstly, the retention time of nitrogen in the cathode will be dramatically reduced under the condition of a nitrogen flow rate higher than 50.0 SCCM. As a result, the crucial adsorption and activation of nitrogen molecules on the catalyst will possibly decrease, thereby hindering the subsequent reaction and reducing the ammonia production rate. Secondly, more water supplied to the cell leads to the water accumulation in the cathode, thus making the hydrogen evolution more serious.

4.3.4. Effect of the cell operation mode

Particularly, the flow cell could be operated in two different modes, constant-gas (CG) mode that NRR and AOR happen on one electrode, and OER and ORR happen on the other electrode, as well as constant-electrode (CE) mode that NRR and ORR happen on one electrode, and OER and AOR happen on the other electrode. Based on the results obtained from the fuel-production mode, the optimal design is that PtAu/C-based electrode and Pt/C-based electrode are employed as the cathode and anode, respectively. Hence, for the CG mode, the PtAu/C-based electrode and Pt/C-based electrode are employed as the anode and cathode in the electricity-generation mode, respectively. On the contrary, for the CE mode, the PtAu/C-based electrode and Pt/C-based electrode are employed as the cathode and anode in the electricity-generation mode, respectively, as shown in Table 1. To determine the optimal operation mode

of this cell, it can be seen from Fig. 12 that although increasing the KOH concentration could enhance the AOR kinetics, and thus the power output is promoted from 0.82 mW cm^{-2} to 1.02 mW cm^{-2} in the CG mode, the CE mode exhibits a boosted cell performance further to 3.31 mW cm^{-2}, suggesting this flow cell mediated by ammonia should adopt the CE operation mode to achieve the promising performance. This phenomenon can be explained by two reasons. On one hand, the Pt/C-based electrode shows better AOR activity than the PtAu/C-based electrode, as evidenced by the CV results in Fig. 7. Therefore, the Pt/C-based electrode performs better than the PtAu/C-based electrode in terms of ammonia oxidation. On the other hand, the ammonia crossover from the anode to cathode results in the serious voltage loss. Hence, the use of less active PtAu/C-based electrode as the cathode in the electricity-generation mode could alleviate the ammonia crossover. Meanwhile, the PtAu/C has been demonstrated to have comparable ORR activity when compared with the Pt/C.

Fig. 13 indicates the round-trip efficiency of this flow cell. The round-trip efficiency is defined by the ratio of the voltages of electricity-generation mode and fuel-production mode at same current density. The applied voltage of the fuel-production mode is unchanged. The CE mode outputs higher voltages than the CG mode. Hence, CE mode achieves superior round-trip efficiency. Since this flow cell is operated at 23 ºC, the round-trip efficiency of is lower than that mediated by hydrogen. It should mention that the kinetics of AOR will be significantly enhanced at increased temperatures, particularly higher than 80 ºC, which dramatically improves the cell performance, and thus the round-trip efficiency.

Table 1 The MEA design of CE and CG modes.

Operation mode		**Anode**	**Membrane**	**Cathode**
Constant electrode	Ammonia-production mode	Pt/C	Fumasep FAS-50	PtAu/C
	Electricity-generation mode	Pt/C		PtAu/C
Constant gas	Ammonia-production mode	Pt/C	Fumasep FAS-50	PtAu/C
	Electricity-generation mode	PtAu/C		Pt/C

5. Conclusions

In this work, a bifunctional electrochemical flow cell integrating ammonia production and electricity generation is developed for renewable energy conversion and storage. This flow cell is able to operate via two modes, i.e., an ammonia-production mode for energy storage in the form of ammonia (via NRR) and an electricity-production mode for energy conversion in the form of electricity (via AOR). In the fuel-production mode, the optimal performance is achieved by employing PtAu/C-based electrode and Pt/C-based electrode as the cathode and anode, respectively. A current density of 10.0 mA cm^{-2} should be applied in case of either the insufficient electron supply required by NRR or the excessively intense side reaction of hydrogen evolution. A nitrogen flow rate of 50.0 SCCM is necessary in case of either the insufficient nitrogen supply required by NRR or the excessive cathode flooding. This flow cell results in a Faradaic efficiency of 2.70% and an ammonia production rate as high as 9.34×10^{-10} mol s^{-1} cm^{-2} at 23 ºC. In the electricity-generation mode, the CE mode leads to an open-circuit voltage of 0.59 V and a peak power density of 3.31 mW cm^{-2} at 23 ºC. A round-trip efficiency of 25.7% is realized with this mode. The developed bifunctional electrochemical flow cell mediated by ammonia represents a promising alternative for mediator hydrogen in terms of storage transmission, distribution, and dispensation costs, as well as safety issues.

Acknowledgement

The work described in this paper was supported by a grant from the Research Grants Council of the Hong Kong Special Administrative Region, China (No. N_PolyU559/21) and a grant from the Shenzhen Science and Technology Innovation Commission (No. JCYJ20210324131406018).

References

[1] Gielen D, Boshell F, Saygin D, Bazilian MD, Wagner N, Gorini R. The role of renewable energy in the global energy transformation. Energy Strategy Rev 2019;24:38-50.

[2] Pan ZF, Chen R, An L, Li YS. Alkaline anion exchange membrane fuel cells for cogeneration of electricity and valuable chemicals. J Power Sources 2017;365:430-45.

[3] Bilgen S. Structure and environmental impact of global energy consumption. Renew Sust Energ Rev 2014;38:890-902.

[4] Deng K, Feng H, Liu D, Chen L, Zhang Y, Li Q. A high-pressure artificial photosynthetic device: pumping carbon dioxide as well as achieving selectivity. J Mater Chem A 2021;9:3961-7.

[5] Dincer I. Renewable energy and sustainable development: a crucial review. Renew Sust Energ Rev 2000;4:157-75.

[6] Pan Z, Bi Y, An L. Performance characteristics of a passive direct ethylene glycol fuel cell with hydrogen peroxide as oxidant. Appl Energy 2019;250:846-54.

[7] Wang Y, Leung DYC, Xuan J, Wang H. A review on unitized regenerative fuel cell technologies, part B: Unitized regenerative alkaline fuel cell, solid oxide fuel cell, and microfluidic fuel cell. Renew Sust Energ Rev 2017;75:775-95.

[8] Gu W, Li S, Liu X, Chen Z, Zhang X, Ma T. Experimental investigation of the bifacial photovoltaic module under real conditions. Renew Energy 2021;173:1111-22.

[9] Jiang H, Wei L, Fan X, Xu J, Shyy W, Zhao T. A novel energy storage system incorporating electrically rechargeable liquid fuels as the storage medium. Sci Bull 2019;64:270-80.

[10] Gabbasa M, Sopian K, Fudholi A, Asim N. A review of unitized regenerative fuel cell stack: Material, design and research achievements. Int J Hydrogen Energy 2014;39:17765-78.

[11] Pan Z, Huang B, An L. Performance of a hybrid direct ethylene glycol fuel cell. Int J Energy Res 2019;43:2583-91.

[12] Pu Z, Zhang G, Hassanpour A, Zheng D, Wang S, Liao S, et al. Regenerative fuel cells: Recent progress, challenges, perspectives and their applications for space energy system. Appl Energy 2021;283:116376.

[13] Wang Y-J, Fang B, Wang X, Ignaszak A, Liu Y, Li A, et al. Recent advancements in the development of bifunctional electrocatalysts for oxygen electrodes in unitized regenerative fuel cells (URFCs). Prog Mater Sci 2018;98:108-67.

[14] Peng X, Taie Z, Liu J, Zhang Y, Peng X, Regmi YN, et al. Hierarchical electrode design of highly efficient and stable unitized regenerative fuel cells (URFCs) for long-term energy storage. Energy Environ Sci 2020;13:4872-81.

[15] Pan Z, Bi Y, An L. Mathematical modeling of direct ethylene glycol fuel cells incorporating the effect of the competitive adsorption. Appl Therm Eng 2019;147:1115-24.

[16] Pan ZF, An L, Zhao TS, Tang ZK. Advances and challenges in alkaline anion exchange membrane fuel cells. Prog Energy Combust Sci 2018;66:141-75.

[17] Lubitz W, Tumas W. Hydrogen: An Overview. Chem Rev 2007;107:3900-3.

[18] Lim A, Jeong H-Y, Lim Y, Kim Jin Y, Park Hee Y, Jang Jong H, et al. Amphiphilic Ti porous transport layer for highly effective PEM unitized regenerative fuel cells. Sci Adv 2021;7:eabf7866.

[19] Pan Z, Zhuang H, Bi Y, An L. A direct ethylene glycol fuel cell stack as air-independent power sources for underwater and outer space applications. J Power Sources 2019;437:226944.

[20] Aasadnia M, Mehrpooya M. Large-scale liquid hydrogen production methods and approaches: A review. Appl Energy 2018;212:57-83.

[21] Lamb KE, Dolan MD, Kennedy DF. Ammonia for hydrogen storage; A review of catalytic ammonia decomposition and hydrogen separation and purification. Int J Hydrogen Energy 2019;44:3580-93.

[22] Abe JO, Popoola API, Ajenifuja E, Popoola OM. Hydrogen energy, economy and storage: Review and recommendation. Int J Hydrogen Energy 2019;44:15072-86.

[23] Pan Z, Khalid F, Tahir A, Esan OC, Zhu J, Chen R, et al. Water flooding behavior in flow cells for ammonia production via electrocatalytic nitrogen reduction. Fundam Res 2021.

[24] Valera-Medina A, Xiao H, Owen-Jones M, David WIF, Bowen PJ. Ammonia for power. Prog Energy Combust Sci 2018;69:63-102.

[25] MacFarlane DR, Cherepanov PV, Choi J, Suryanto BHR, Hodgetts RY, Bakker JM, et al. A Roadmap to the Ammonia Economy. Joule 2020;4:1186-205.

[26] Zhao Y, Setzler BP, Wang J, Nash J, Wang T, Xu B, et al. An Efficient Direct Ammonia Fuel Cell for Affordable Carbon-Neutral Transportation. Joule 2019;3:2472-84.

[27] Hu C, Zhang L, Gong J. Recent progress made in the mechanism comprehension and design of electrocatalysts for alkaline water splitting. Energy Environ Sci 2019;12:2620-45.

[28] Mukherjee S, Cullen DA, Karakalos S, Liu K, Zhang H, Zhao S, et al. Metal-organic framework-derived nitrogen-doped highly disordered carbon for electrochemical ammonia synthesis using N2 and H2O in alkaline electrolytes. Nano Energy 2018;48:217-26.

[29] Li Y, Pillai HS, Wang T, Hwang S, Zhao Y, Qiao Z, et al. High-performance ammonia oxidation catalysts for anion-exchange membrane direct ammonia fuel cells. Energy Environ Sci 2021;14:1449-60.

[30] Pan ZF, An L, Wen CY. Recent advances in fuel cells based propulsion systems for unmanned aerial vehicles. Appl Energy 2019;240:473-85.

[31] Liang L, Vladimir F, Ge J, Liu C, Xing W. Highly active PtAu alloy surface towards selective formic acid electrooxidation. J Energy Chem 2019;37:157-62.

[32] Pan Z, Bi Y, An L. A cost-effective and chemically stable electrode binder for alkaline-acid direct ethylene glycol fuel cells. Appl Energy 2020;258:114060.

[33] Li G, Yu Y, Pan Z, An L. Two-Dimensional Layered SnO2 Nanosheets for Ambient Ammonia Synthesis. ACS Appl Energy Mater 2020;3:6735-42.

[34] Depciuch J, Stec M, Klebowski B, Baran J, Parlinska-Wojtan M. Platinum–gold nanoraspberries as effective photosensitizer in anticancer photothermal therapy. J Nanobiotechnology 2019;17:107.

[35] Bhunia K, Chandra M, Khilari S, Pradhan D. Bimetallic PtAu Alloy Nanoparticles-Integrated g-C3N4 Hybrid as an Efficient Photocatalyst for Water-to-Hydrogen Conversion. ACS Appl Mater Interfaces 2019;11:478-88.

[36] Xue Q, Bai X-Y, Zhao Y, Li Y-N, Wang T-J, Sun H-Y, et al. Au core-PtAu alloy shell nanowires for formic acid electrolysis. J Energy Chem 2022;65:94-102.

[37] Yao Y, Zhu S, Wang H, Li H, Shao M. A Spectroscopic Study on the Nitrogen Electrochemical Reduction Reaction on Gold and Platinum Surfaces. J Am Chem Soc 2018;140:1496-501.

Figures:

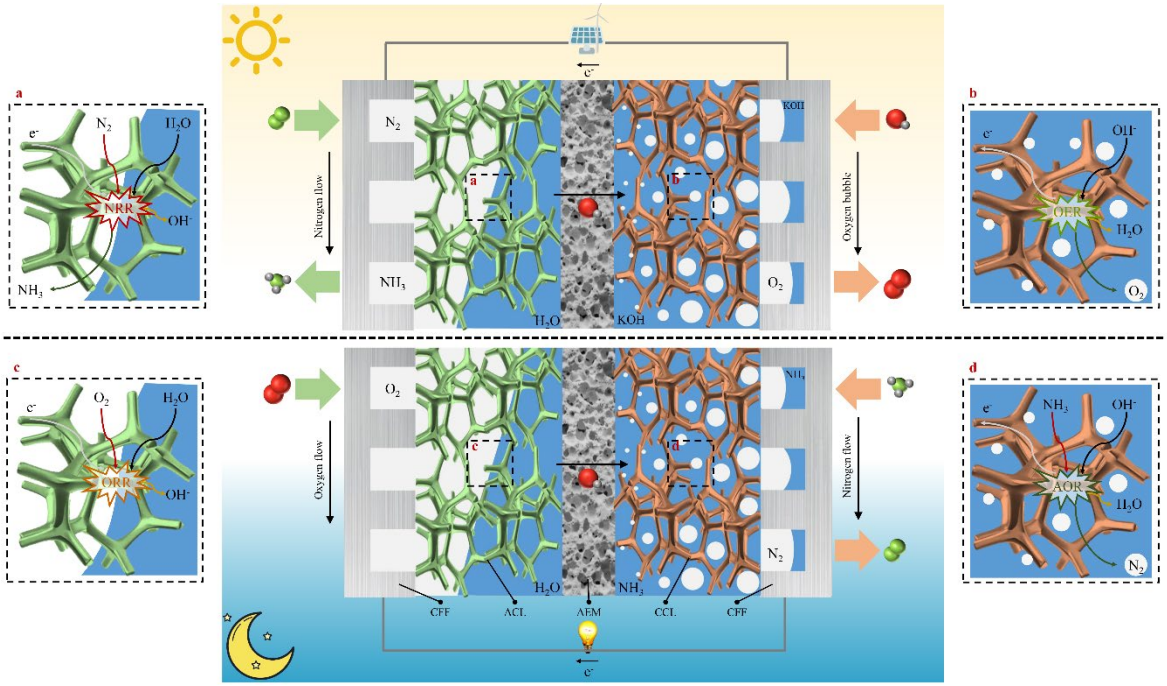

Fig. 1 Working principle of the bifunctional electrochemical flow cell.

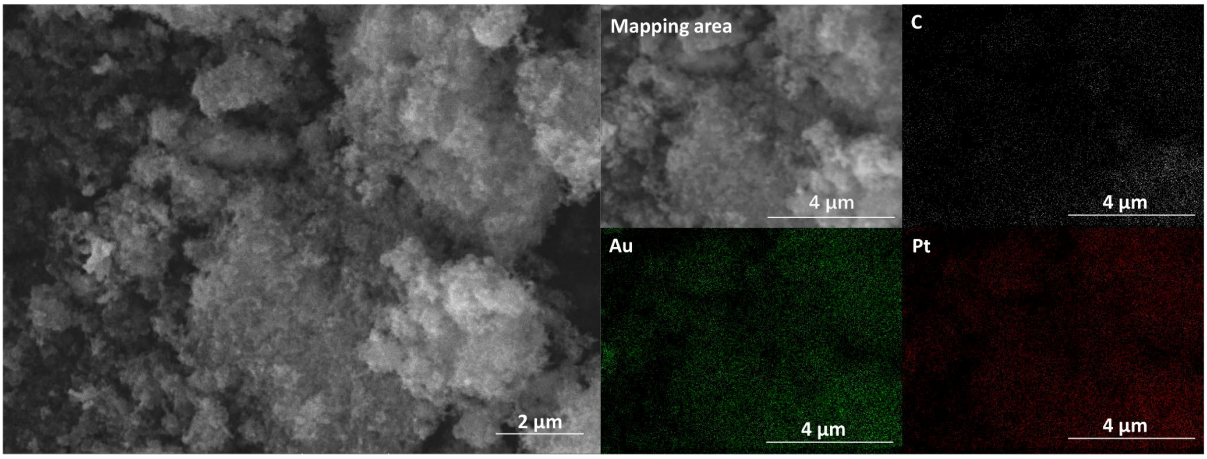

Fig. 2 SEM image and element mapping of prepared PtAu/C.

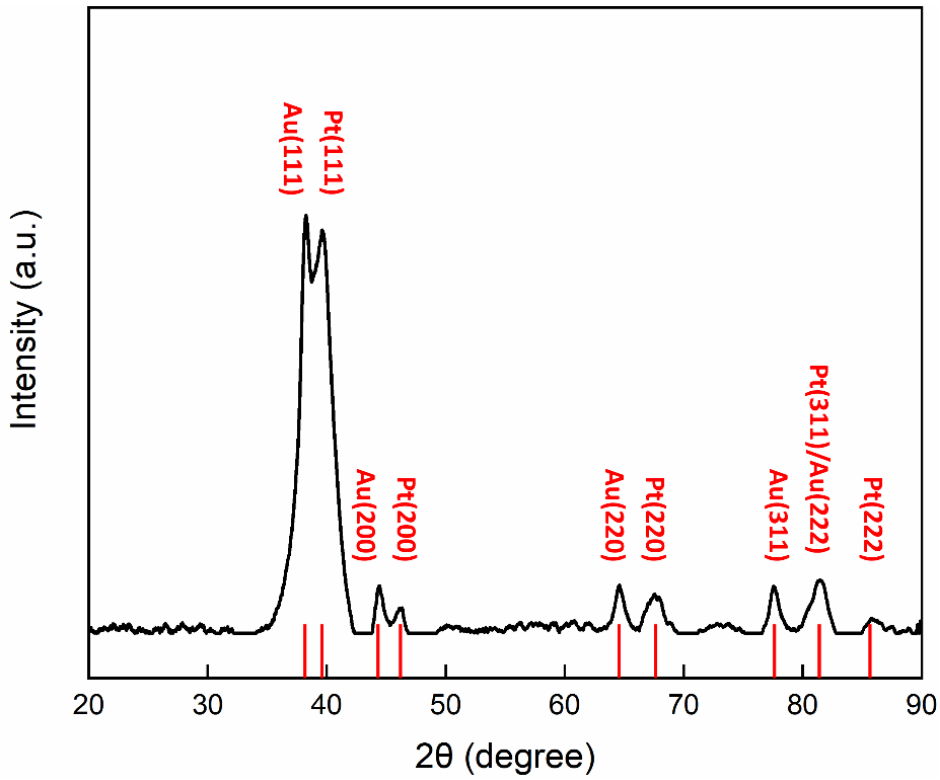

Fig. 3 XRD pattern of prepared PtAu/C.

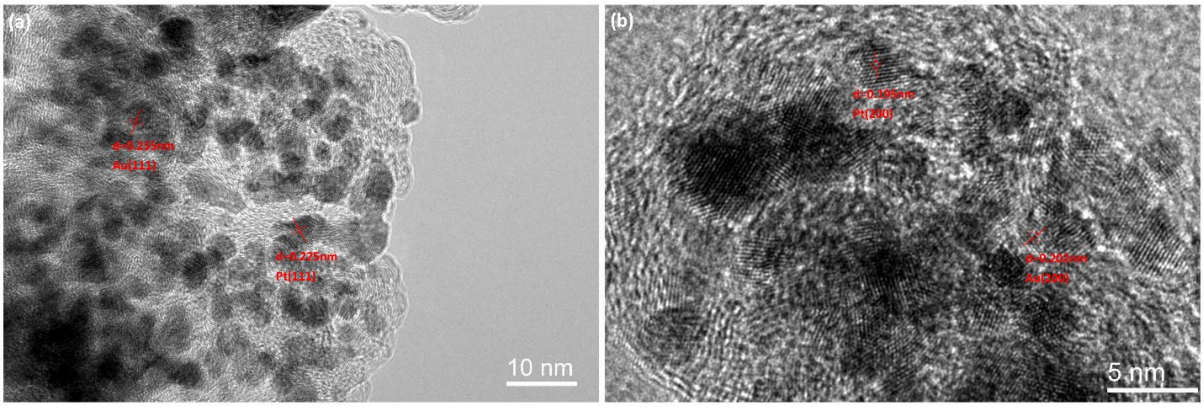

Fig. 4 (a) TEM images with (111) facets and (b) TEM images with (200) facets.

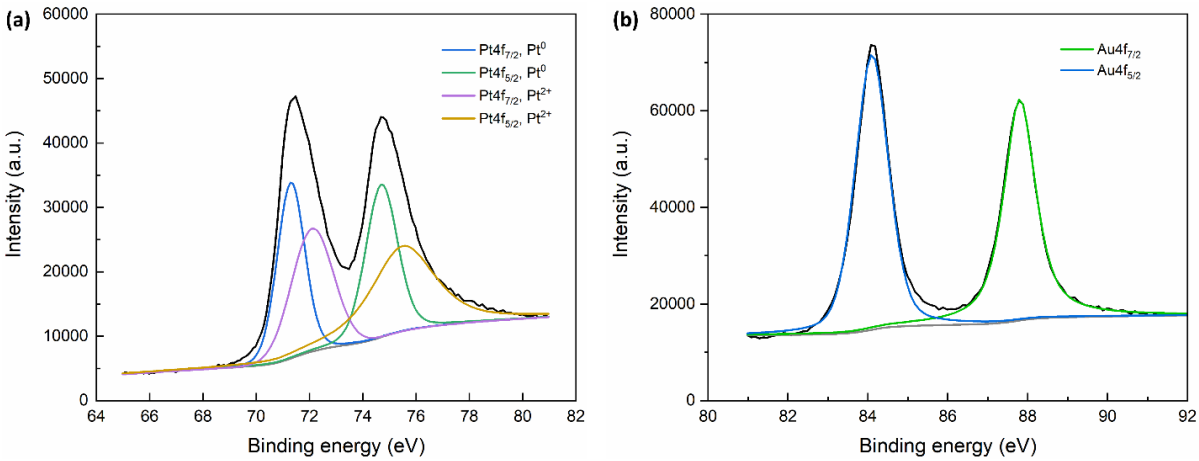

Fig. 5 XPS spectra of Pt 2f and Au 2f.

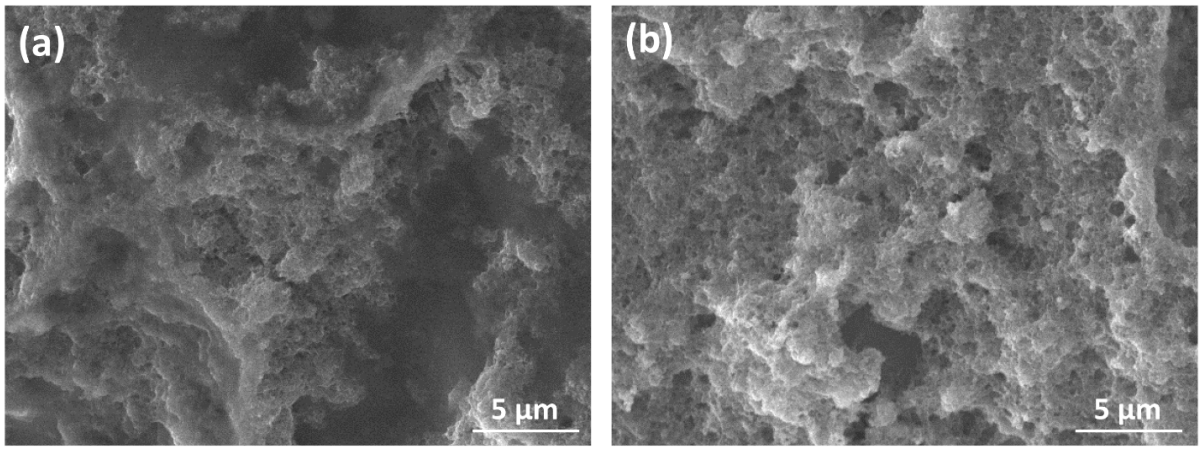

Fig. 6 SEM images of (a) Pt/C-based electrode and (b) PtAu/C-based electrode.

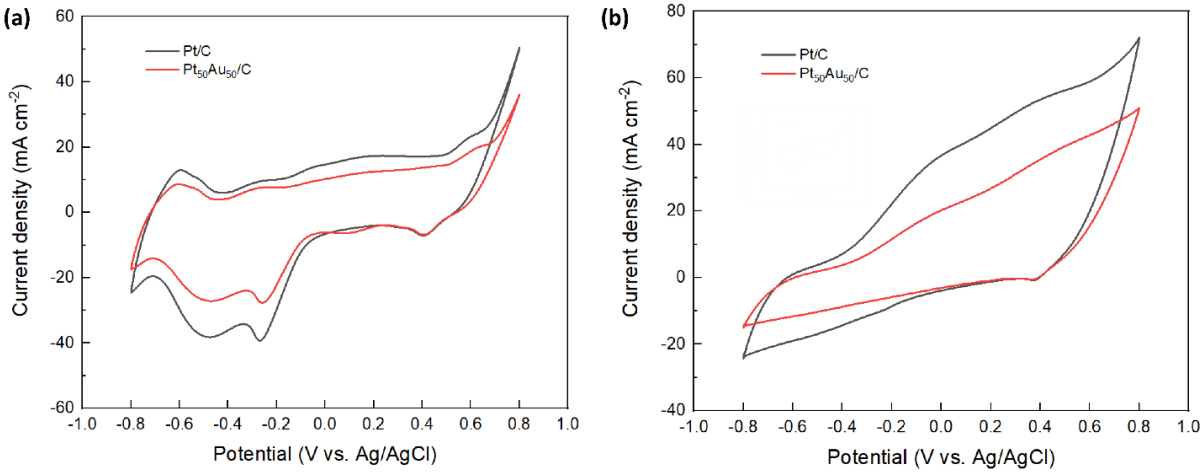

Fig. 7 CV results of two electrodes in (a) 1.0 M KOH solution and (b) 1.0 M NH_3 and 1.0 M KOH solution.

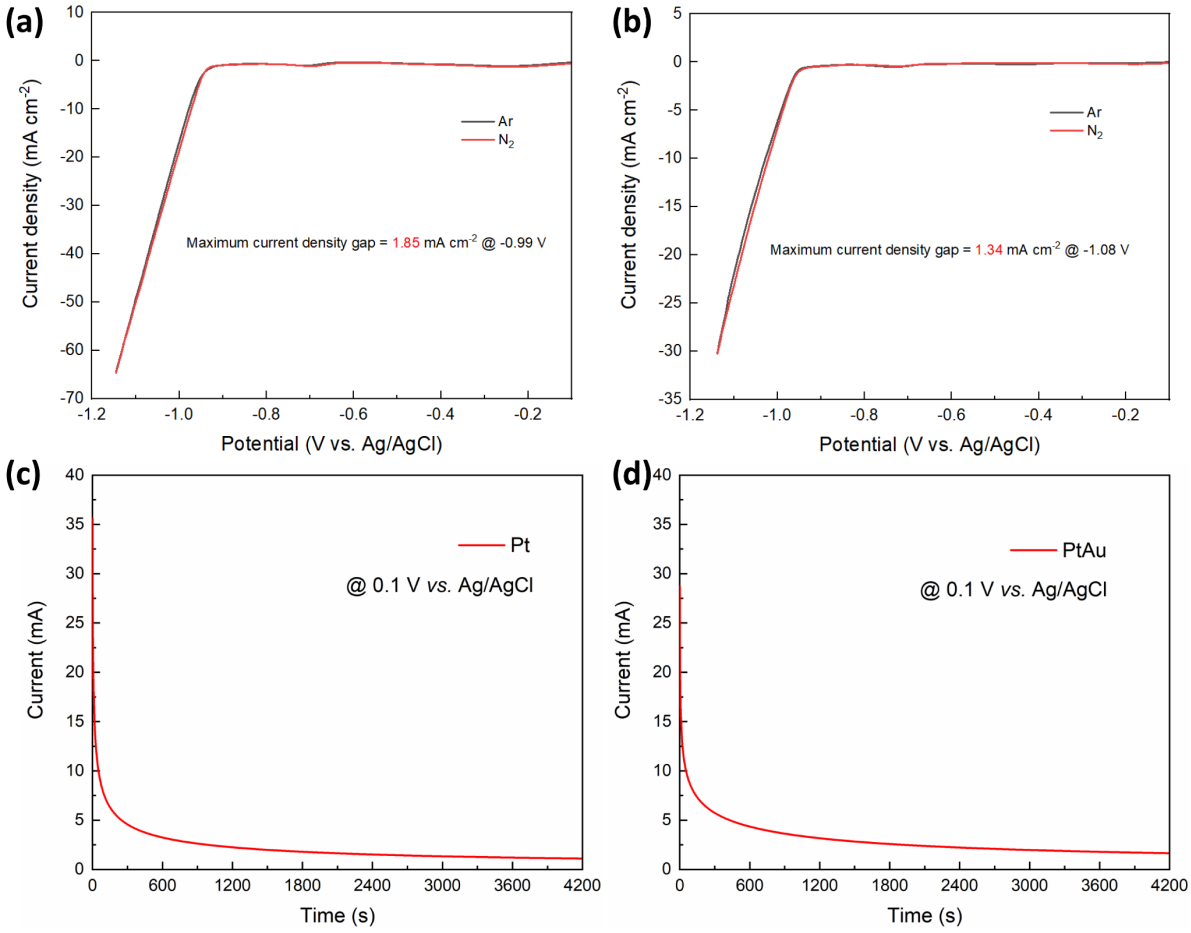

Fig. 8 LSV results of (a) Pt/C-based electrode and (b) PtAu/C-based electrode, and CA results of (c) Pt and (d) PtAu.

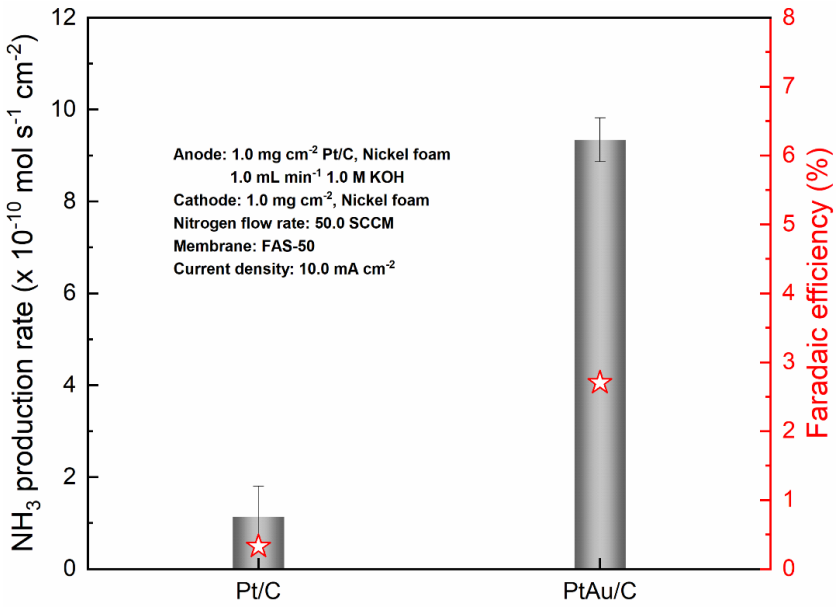

Fig. 9 Electrochemical ammonia production of two electrodes.

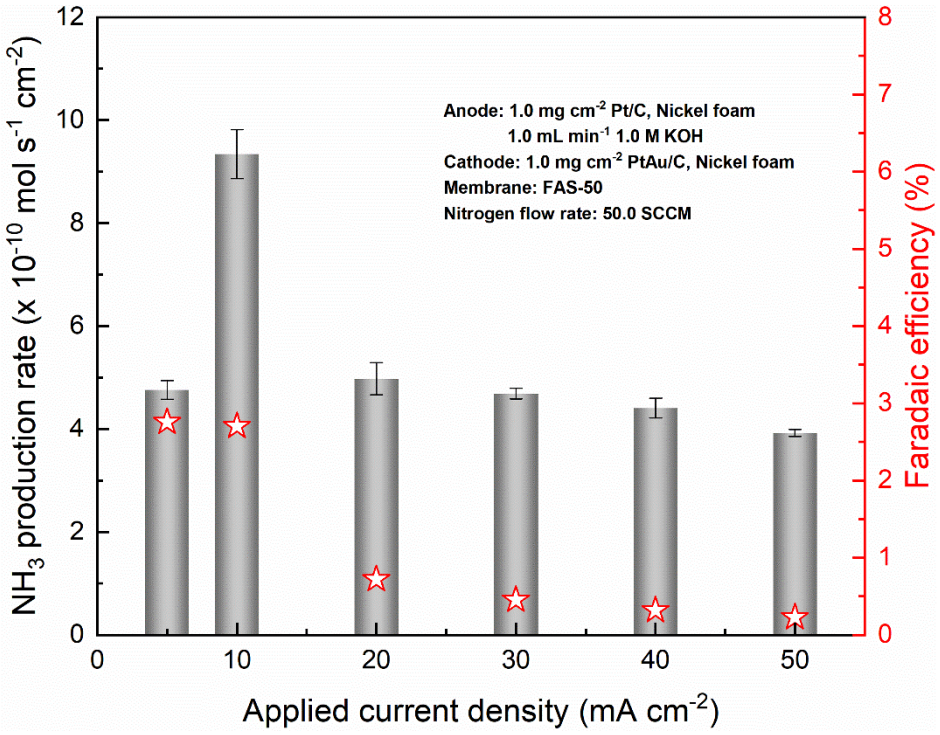

Fig. 10 Electrochemical ammonia production at different applied current densities.

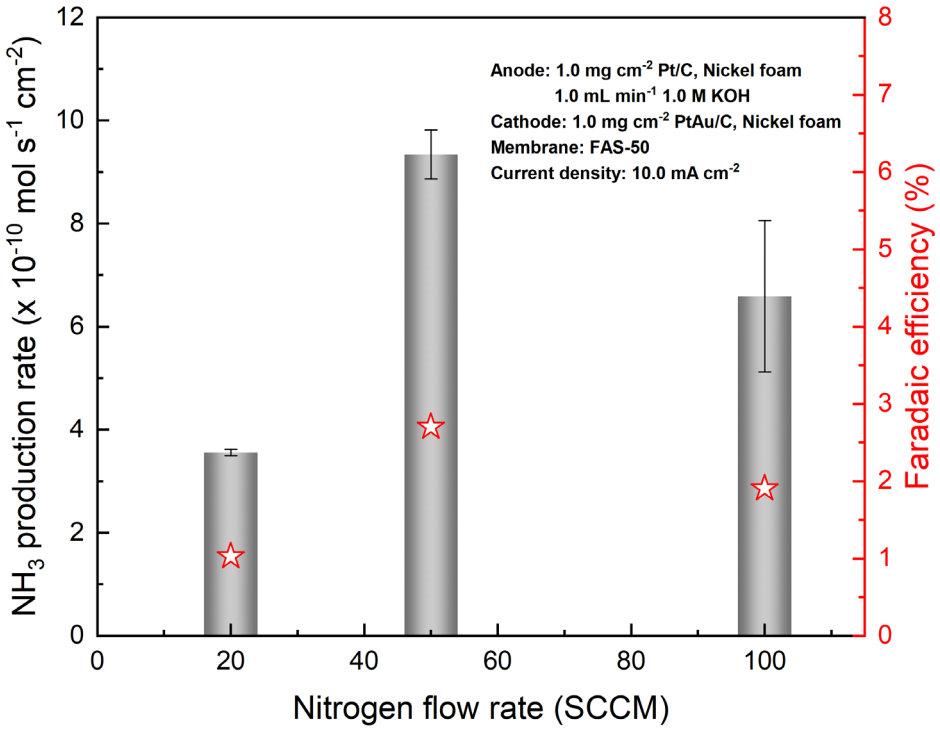

Fig. 11 Electrochemical ammonia production at different nitrogen flow rates.

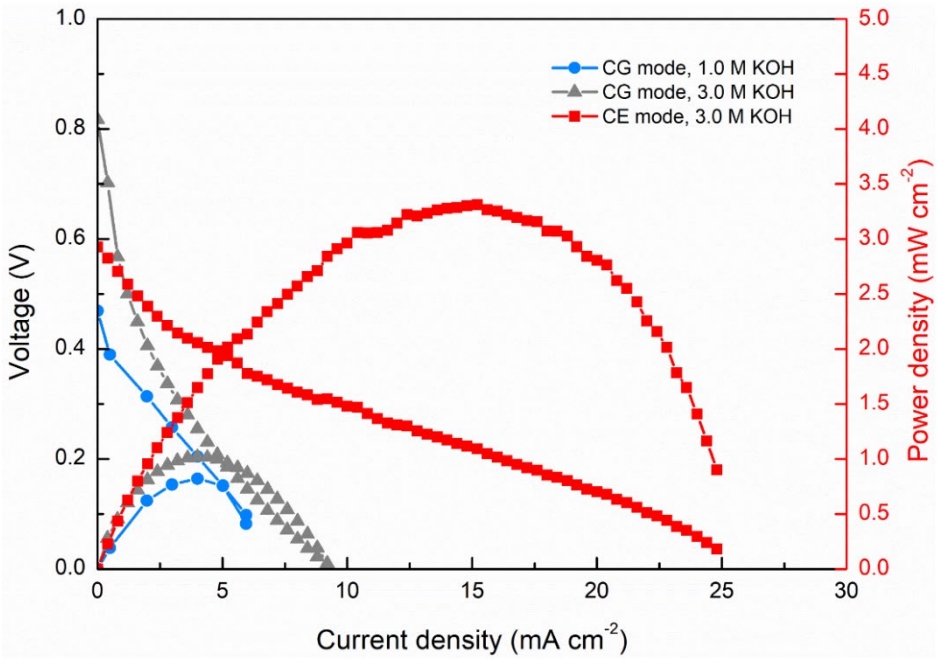

Fig. 12 Polarization and power density curves of different operation modes.

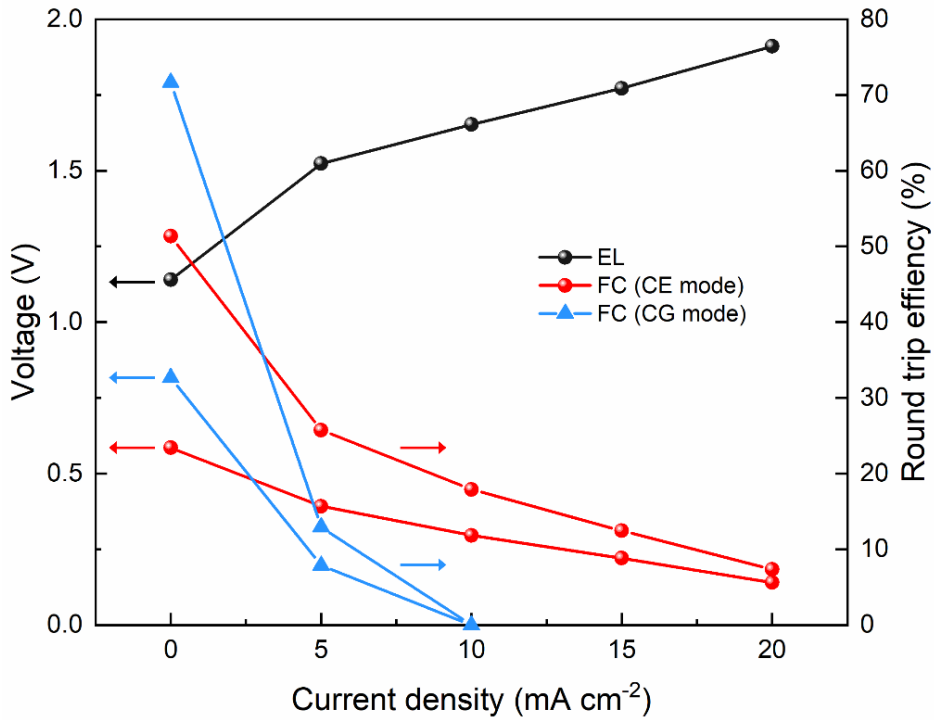

Fig. 13 Round-trip efficiency of the bifunctional electrochemical flow cell.

Highlights

- A flow cell integrating ammonia production and electricity generation is developed.
- It produces NH_3 at a rate of 9.34×10^{-10} mol s^{-1} cm^{-2} with an efficiency of 2.70%.
- It exhibits a voltage of 0.59 V and a peak power density of 3.31 mW cm^{-2} at 23 ^{o}C.
- A round trip efficiency of 25.7% is realized with the constant-electrode mode.

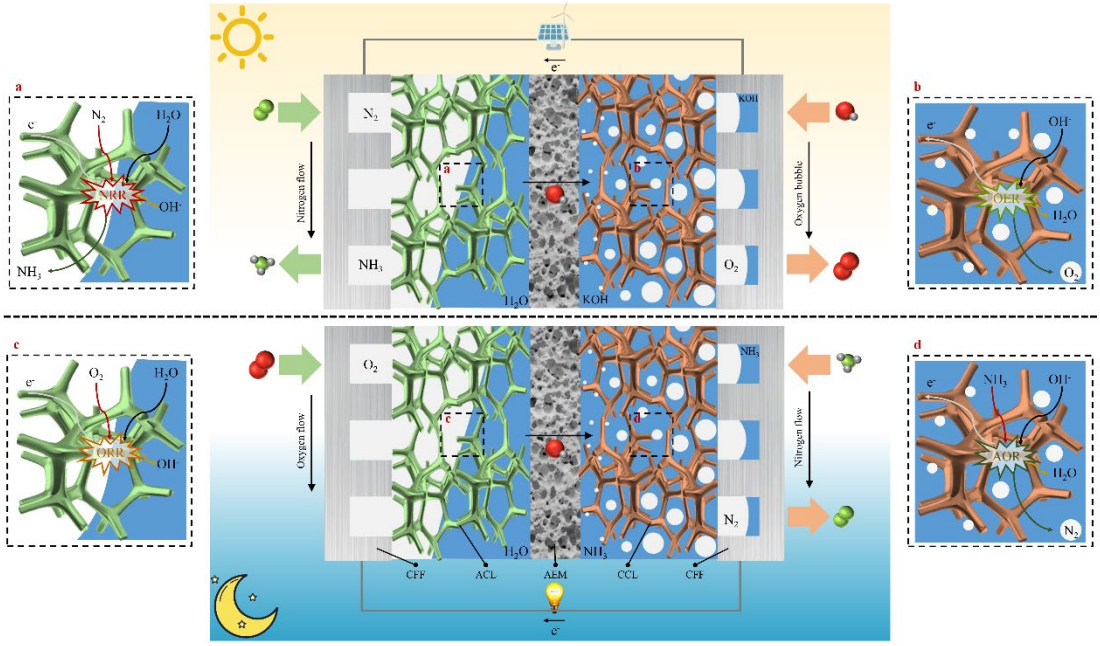
a
e⁻
N₂
H₂O
NRR
OH⁻
NH₃
b
e⁻
OH⁻
OER
H₂O
O₂
N₂
KOH
Nitrogen flow
Oxygen bubble
NH₃
O₂
H₂O
KOH
c
e⁻
O₂
H₂O
ORR
OH⁻
d
e⁻
NH₃
OH⁻
AOR
H₂O
N₂
O₂
NH₃
Oxygen flow
Nitrogen flow
N₂
H₂O
NH₃
CFF
ACL
AEM
CCL
CFF
e⁻